

RESEARCH ARTICLE

10.1002/2015JD024018

Key Points:

- Sea ice north of Greenland has BC mixing ratios of typically 3–6 ng/g
- Mixing ratios of BC in sea ice north of Greenland vary but show no trend from 2008 to 2013
- Interannual variations show some relationship to air mass source region

Correspondence to:

S. J. Doherty,
sarahd@atmos.washington.edu

Citation:

Doherty, S. J., M. Steele, I. Rigor, and S. G. Warren (2015), Interannual variations of light-absorbing particles in snow on Arctic sea ice, *J. Geophys. Res. Atmos.*, 120, 11,391–11,400, doi:10.1002/2015JD024018.

Received 29 JUL 2015

Accepted 16 OCT 2015

Accepted article online 21 OCT 2015

Published online 10 NOVEMBER 2015

Interannual variations of light-absorbing particles in snow on Arctic sea ice

Sarah J. Doherty¹, Michael Steele², Ignatius Rigor², and Stephen G. Warren³

¹Joint Institute for the Study of the Atmosphere and Ocean, University of Washington, Seattle, Washington, USA, ²Polar Science Center, Applied Physics Laboratory, University of Washington, Seattle, Washington, USA, ³Department of Atmospheric Sciences, University of Washington, Seattle, Washington, USA

Abstract Samples of snow on sea ice were collected in springtime of the 6 years 2008–2013 in the region between Greenland, Ellesmere Island, and the North Pole (82°N–89°N, 0°W–100°W). The meltwater was passed through filters, whose spectral absorption was then measured to determine the separate contributions by black carbon (BC) and other light-absorbing impurities. The median mixing ratio of BC across all years' samples was $4 \pm 3 \text{ ng g}^{-1}$, and the median fraction of absorption due to non-BC absorbers was $36 \pm 11\%$. Variances represent both spatial and interannual variability; there was no interannual trend in either variable. The absorption Ångström exponent, however, decreased with latitude, suggesting a transition from dominance by biomass-burning sources in the south to an increased influence by fossil-fuel-burning sources in the north, consistent with earlier measurements of snow in Svalbard and at the North Pole.

1. Introduction

The presence of black carbon (BC), organic carbon, or mineral dust in snow causes a reduction of the snow's albedo [e.g., Warren and Wiscombe, 1980; Flanner *et al.*, 2007]. Quantification of this reduction requires both modeling of radiative transfer and measurement of impurities in the snow. Since the 1980s, the role of black carbon in the Arctic region has been of particular interest because of the springtime "Arctic haze"; more recently interest has intensified because of the search for causes of the dramatic decline of Arctic sea ice. Measurements of the near-surface air at Alert (82.5°N, 62°W) have shown a statistically significant decline in BC concentrations of about 2–3% yr⁻¹ from 1990 to 2007 [Gong *et al.*, 2010]. Correspondingly, the BC content of Arctic snow during 2005–2010 [Doherty *et al.*, 2010, Table 9] was found to be smaller than that measured by a very similar method 25 years earlier [Clarke and Noone, 1985], but because of differences in the method and the small number of samples from the earlier study, we cannot be sure that the difference is significant. In any case, the BC present in the snow does lower the albedo below what it would be for pure snow, and there is also the risk that the BC content will increase in the future as a result of increased ship traffic in the Arctic or enhanced transport of pollution from industrializing regions of the middle latitudes. For this reason it is useful to monitor BC in snow at a few locations in the Arctic.

Doherty *et al.* [2010, hereafter "D10"] reported the results of a broad-area survey of BC and other light-absorbing particles in Arctic snow and sea ice, and these data are being used, along with other measurements of BC in snow, to test modeled mixing ratios of BC in snow [Lund and Berntsen, 2011; Skeie *et al.*, 2011; Dou *et al.*, 2012; Bond *et al.*, 2013; Boucher *et al.*, 2013; Lee *et al.*, 2013; Jiao *et al.*, 2014; Qian *et al.*, 2014] and to adjust modeled climate forcing by BC in snow and ice [e.g., Bond *et al.*, 2013; Boucher *et al.*, 2013; Qian *et al.*, 2014]. An advantage of the D10 study is that a single sampling protocol and measurement technique was used across all sampling sites so that results from different regions are comparable. A disadvantage is that each site was sampled only once. Different regions (Greenland, Canada, Russia, and Scandinavia) were sampled in different years. With no measure of the interannual variability of the mixing ratio of BC in snow, it is difficult to determine the representativeness of the samples collected in the Arctic survey.

Here we report results using the same method as D10 but for snow samples collected from one Arctic region in the same season (April–May) in each of the 6 years 2008–2013. The mixing ratios of BC and other light-absorbing particles in snow are of particular interest in spring, because this is when both sea ice extent [Gloersen *et al.*, 1992] and snow depth [Warren *et al.*, 1999] are near their maxima and the incident solar radiation is strong and increasing. As temperatures warm later in spring, these light-absorbing particles trigger a positive feedback: Melt is accelerated in snow containing light-absorbing particles due to its lowered

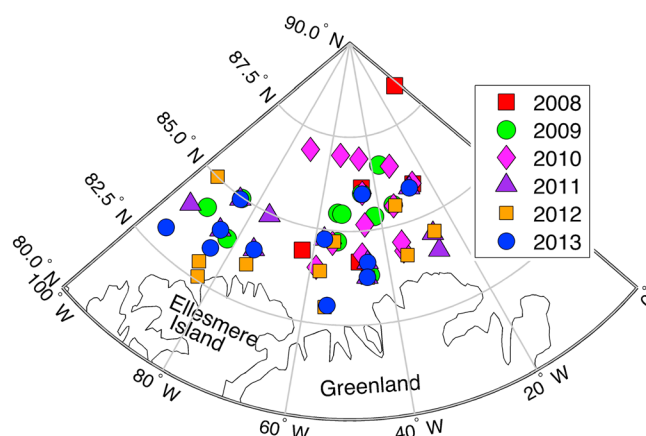


Figure 1. Locations of sampling sites in each year 2008–2013. In 2008, four samples were gathered at the northernmost site (88.345°N, 3.407°W); at all other locations, there is only one filter sample per site. In 2013, two samples per site were obtained, but the sample sizes were small so they were combined during filtration.

the Lincoln Sea forms locally, but much of it advects into the region from the north via the Transpolar Drift Stream (TDS), which flows across the North Pole from Siberian coastal regions. The exact geographic origin of the TDS varies interannually depending on the wind forcing. In years with a strong negative Arctic Oscillation (AO) index, the TDS starts near the Laptev Sea, whereas its origin shifts eastward into the East Siberian Sea for a strong positive AO index [Steele *et al.*, 2004].

The sampling locations are shown in Figure 1. All samples presented here are of snow on sea ice. Given the time of year (early May) and high latitude, it is expected that the snow sampled had remained frozen since falling on the sea ice. Thus, measured snow particulate mixing ratios will be influenced by wet deposition, dry deposition, and snow sublimation but probably not by melting.

Below we present interannual variations in the BC mixing ratio in snow, the absorption Ångström exponent (\hat{A}_{tot}) of all particulate impurities, and the fraction of solar absorption by non-BC components of the particles. \hat{A}_{tot} is a measure of the color of snow particles: Gray particles have low values of \hat{A}_{tot} ; browner/redder particles have higher values of \hat{A}_{tot} . Thus, \hat{A}_{tot} varies with particle type and often with source. Interannual variations in the particle source regions are also explored using back trajectories of sea ice location coupled with air mass back trajectories.

2. Methods

The sampling and measurement techniques used in our analysis follow those of D10 and so will be described only briefly here. Most samples collected through 2012 were of surface snow only, with each sample typically from the surface to ~15–20 cm depth. Total snowpack depth was usually 15 cm or more, but where it was shallower the total snowpack depth was sampled. In 2013, however, filter samples represent the entire snowpack, not just the surface snow. In all years, care was taken not to scrape the surface of the sea ice, so samples should be of snow only. Sample 13.9 in 2013 (Table 1) was an exception: Total snow depth was less than 1 cm, and it is possible that the sample contained some sea ice. Notably, this sample, with estimated BC of 16 ng g^{-1} , is dirtier than all but one other sample collected during the 6 years.

In 2008 and 2009, samples were collected in glass jars using clean utensils or by pushing the jars vertically into the snow (Figure 2). The glass jars were then capped and placed in plastic bags for protection. These samples melted in transit, then they were refrozen for storage before being intentionally melted for filtration. Some or all of the melted water leaked from the jars and then refroze in the plastic bags. For these samples it is possible that there was some particle loss to the walls of the plastic bags [Doherty *et al.*, 2010].

In 2010, samples were collected in Whirlpak bags and in 2011–2013 they were collected in food grade bags placed in Whirlpak bags for protection from puncture. All samples in 2010–2013 were kept frozen until they were intentionally melted in the laboratory, then filtered.

albedo; the loss of snow water with melt generally leads to enhanced concentrations of particles at the snow surface [e.g., Conway *et al.*, 1996; Xu *et al.*, 2012; Doherty *et al.*, 2013]; snow albedo is reduced further; melt is further accelerated; and eventually the darker underlying surface (in this case, sea ice and then ocean) is exposed [e.g., Flanner *et al.*, 2007; Bond *et al.*, 2013].

The sampling area for this study is the sea ice pack of the greater Lincoln Sea and north into the Arctic Ocean, north of Ellesmere Island (Canada) and Greenland. This region lies just upstream of ocean and sea ice outflows into Nares Strait (west of northern Greenland) and Fram Strait (east of northern Greenland). Some sea ice in

Table 1. Snow Samples Collected in the Switchyard Region, 2008–2013. Total Snowpack Depth was Recorded Only in 2009 and 2013^a

Sample No.	Date	Lat (°N)	Lon (°W)	C_{BC}^{est} (ng g ⁻¹)	Comments
2008					
8.1	4/20	88.35	3.41	4.8	all 2008 samples collected in glass jars, stored in plastic bags; samples melted in transit, leaked into bags, and were refrozen.
8.2	4/20	88.35	3.41	6.1	
8.3	4/20	88.35	3.41	6.4	
8.4	4/20	84.36	63.00	9.8	
8.5	5/6	84.18	47.51	5.5	
8.6	5/4	85.90	25.80	5.2	
8.7	5/2	86.14	45.34	5.8	
2009					
9.1	5/3	85.35	41.82	4.1	all 2009 samples collected in glass jars, stored in plastic bags; samples melted in transit, leaked into bags, and were refrozen.
9.2	5/3	84.72	53.61	3.4	
9.3	5/4	83.82	44.87	2.4	
9.4	5/8	86.67	36.53	6.5	
9.5	5/8	85.47	54.07	8.9	
9.6	5/19	85.55	34.89	11.8	
9.7	5/19	85.45	52.64	5.1	
9.8	5/14	85.99	45.47	2.7	
9.9	5/15	84.22	91.14	8.5	
9.10	5/17	84.97	84.95	12.2	
9.11	5/17	83.87	82.22	10.7	
2010					
10.1	5/5	84.30	35.35	3.6	all 2010 samples collected in Whirlpak bags
10.2	5/5	84.30	35.35	4.3	
10.3	5/8	84.54	35.32	4.3	
10.4	5/8	84.54	35.32	3.9	
10.5	5/8	85.16	45.23	2.7	
10.6	5/15	85.16	45.23	4.2	
10.7	5/15	86.00	45.22	3.5	
10.8	5/15	86.56	32.18	3.2	
10.9	5/16	85.52	34.88	5.4	
10.10	5/16	85.52	34.88	2.4	
10.11	5/16	85.92	26.00	3.9	
10.12	5/17	85.92	26.00	3.8	
10.13	5/17	86.92	45.50	2.3	
10.14	5/17	86.92	45.50	3.1	
10.15	5/17	84.37	46.64	3.4	
10.16	5/5	84.37	46.64	4.0	
10.17	5/5	84.67	54.93	2.8	
10.18	5/8	84.67	54.93	2.3	
10.19	5/8	83.98	58.61	3.5	
10.20	5/8	83.98	58.61	2.8	
10.21	5/15	87.01	54.73	3.7	
10.22	5/15	87.01	54.73	2.9	
10.23	5/15	86.99	70.36	4.4	
10.24	5/16	86.99	70.36	3.4	
2011					
11.1	4/30	84.755	57.381	2.8	all 2011 samples collected in food grade bags
11.2	5/1	85.843	27.613	5.7	
11.3	5/1	84.157	45.309	5.2	
11.4	5/2	84.938	85.135	1.8	
11.5	5/2	84.942	74.997	2.2	
11.6	5/2	83.956	75.016	1.9	
11.7	5/5	84.011	26.471	15.9	
11.8	5/5	84.486	26.281	10.6	
11.9	5/6	83.979	94.829	3.1	
11.10	5/8	83.766	45.652	4.2	
11.11	5/9	83.966	84.869	2.9	
2012					
12.1	5/3	84.718	54.571	2.7	two samples combined

Table 1. (continued)

Sample No.	Date	Lat (°N)	Lon (°W)	C_{BC}^{est} (ng g ⁻¹)	Comments
12.2	5/3	83.899	57.519	2.4	all 2012 samples collected in food grade bags
12.3	5/3	83.899	57.519	2.5	
12.4	5/5	85.520	34.301	1.8	
12.5	5/8	82.956	55.475	7.1	
12.6	5/10	84.523	25.632	2.9	
12.7	5/10	84.523	25.632	4.0	
12.8	5/10	84.166	34.662	1.3	
12.9	5/10	83.756	45.567	2.1	
12.10	5/12	85.005	94.858	4.1	
12.11	5/16	82.603	83.290	6.1	
12.12	5/16	82.957	84.831	2.0	
12.13	5/16	83.513	75.220	2.0	
2013					
13.1	4/30	83.090	95.141	4.7	all 2013 samples collected in food grade bags
13.2	5/2	84.755	57.381	5.7	
13.3	5/2	85.843	27.613	9.3	
13.4	5/3	85.977	45.366	5.1	
13.5	5/3	84.157	45.309	4.1	
13.6	5/7	83.421	84.436	6.2	
13.7	5/11	83.005	55.024	9.3	
13.8	5/13	84.938	85.135	9.1	
13.9	5/13	83.956	75.016	15.7	
13.10	5/15	83.766	45.652	5.8	
13.11	5/15	83.966	84.869	7.3	

^aIn 2010, total snow depth at the sampling sites varied in the range of 15–30 cm. In 2008–2012, samples were of the top 15–20 cm of the snowpack only. In 2013, samples were collected from two depths which, together, covered the entire snowpack depth. Because they were small, these samples were combined before filtration and analysis.

In the laboratory, samples were melted rapidly in a glass beaker in a microwave oven. Immediately after melting, the water from each sample was drawn through a Nuclepore filter of pore size 0.4 μm. The capture efficiency of these filters for our Arctic field samples varied between 70% and 100% and on average was 85%, so a 15% undercatch correction was applied to all samples, as in D10.



Figure 2. Samples being collected in glass jars in 2009 in the Switchyard region.

Filters were optically analyzed using the Integrating Sphere, Integrating Sandwich (ISSW) spectrophotometer [Grenfell *et al.*, 2011], modified such that the integrating sandwich was replaced with a second integrating sphere [see Doherty *et al.*, 2014, section 2.2]. The ISSW measures spectrally resolved absorption across the wavelength range of 450–700 nm, and from this we extrapolate absorption down to 300 nm and up to 750 nm [Doherty *et al.*, 2010]. As described in detail by Grenfell *et al.* [2011] and D10, the following parameters are then derived:

\hat{A}_{tot} : The absorption Ångström exponent of all insoluble particles in snow calculated as a linear fit to the logarithm of spectral absorption versus the logarithm of wavelength 450–600 nm.

C_{BC}^{est} (ng g^{-1}): The estimated mixing ratio of BC in the snow.

C_{BC}^{equiv} (ng g^{-1}): The amount of BC that would be needed to produce the absorption of solar energy, integrated across 300–750 nm, by all insoluble particles in snow.

f_{non-BC}^{est} : The estimated fraction of solar energy absorption 300–750 nm due to insoluble, non-BC components of the particles in snow.

Our estimate of the mixing ratio of BC in snow, C_{BC}^{est} , and the fraction of non-BC absorption, f_{non-BC}^{est} , are based on apportioning absorption to BC and non-BC particulate components. Using the measured absorption Ångström exponent for all particles, \hat{A}_{tot} , we apportion the absorption in the 450–600 nm band to BC and non-BC components using assumed absorption Ångström exponents for each: $\hat{A}_{BC} = 1.1$ and $\hat{A}_{non-BC} = 5.0$, as in D10. An analysis of the uncertainty of this apportionment can be found in D10 (see their Figure 16 and associated discussion). For the range of values of \hat{A}_{tot} measured here (1.8–2.3), the uncertainty in C_{BC}^{est} is between 20% (for $\hat{A}_{tot} = 1.8$) and 40% (for $\hat{A}_{tot} = 2.3$), based on allowing \hat{A}_{BC} to vary 0.8–1.9 and \hat{A}_{non-BC} to vary 3.5–7.0. A recent study indicates that BC particles in snow maybe larger than in the atmosphere [Schwarz *et al.*, 2013], in which case \hat{A}_{BC} is likely lower than 1.1 [e.g., see Clarke *et al.*, 1987, Figure 6e and Dang *et al.*, 2015, Figure 3e]; if so, our values of C_{BC}^{est} are biased high. However, assuming the actual value of \hat{A}_{BC} and \hat{A}_{non-BC} do not vary from year to year, any errors in our assumed values of \hat{A}_{BC} and \hat{A}_{non-BC} should not translate into spurious trends in C_{BC}^{est} .

After estimating the amount of absorption allocated to BC in the middle of the 450–600 nm band (525 nm), we extrapolate BC absorption to 700 nm by again assuming the absorption Ångström exponent for BC is 1.1. The 650–700 nm wavelength absorption allocated to BC is then converted to a filter mass loading ($\mu\text{g cm}^{-2}$) using a set of calibration standards. The calibration standards are a set of filters with gravimetrically determined loadings of a synthetic BC, fullerene (Alfa Aesar, Inc., Ward Hill, MA, USA). The loading of BC on the filter is converted to a mixing ratio of BC in snow (C_{BC}^{est}) based on the exposed area of the filter and the volume of meltwater filtered. Similarly, solar irradiance-weighted integrated absorption 300–750 nm is converted to an equivalent BC mass filter loading then to an equivalent BC mass mixing ratio in snow (C_{BC}^{equiv}).

Thus, the mass mixing ratios C_{BC}^{est} and C_{BC}^{equiv} quantify the masses of fullerene that would be needed to produce the amount of light absorption allocated to BC only (C_{BC}^{est}) and to all particles (C_{BC}^{equiv}). Both depend on the mass absorption efficiency of fullerene, which we estimate to be 8.9, 7.2, and $6.5 \text{ m}^2 \text{ g}^{-1}$ at 450, 550, and 600 nm, respectively.

It is important to note that C_{BC}^{equiv} is a metric (expressed as a BC mass mixing ratio) for the total particulate spectral absorption in snow, not a measure of the amount of BC in the snow. Snow containing no BC, but containing other types of light-absorbing particles such as dust, would have $C_{BC}^{equiv} > 0$. The product of C_{BC}^{equiv} and f_{non-BC}^{est} is a metric for the amount of non-BC particulate absorption, also expressed as a BC mass mixing ratio. This product can be compared directly to the estimated BC mass mixing ratio (C_{BC}^{est}) to indicate the relative roles of the two in darkening the snow.

Components of uncertainty in the derived parameters are taken from D10. For C_{BC}^{est} they include: 10% for system calibration; 15% for the correction to particulate undercatch on the filters (i.e., allowing for 0–30% undercatch); 20% uncertainty in the mass absorption efficiency of black carbon used to convert measured absorption to a BC mass mixing ratio; and an uncertainty in the apportionment of absorption to BC and non-BC components that depends on \hat{A}_{tot} (see Figure 16a of D10). For the samples reported here, this last source of uncertainty varied between 20% and 35%. Uncertainty in f_{non-BC}^{est} is analogously based on Figure 16b of D10. Sources of uncertainty in C_{BC}^{est} for individual samples are assumed to be uncorrelated and normally distributed and so are added in quadrature. Uncertainties in the means across all samples in a given year are reduced by the square root of the number of samples in that year.

3. Results

The mixing ratio of BC in snow (C_{BC}^{est}) in the Switchyard region varies both spatially within a year and interannually, but there is no trend in C_{BC}^{est} over the period 2008–2013 (Figure 3a). C_{BC}^{est} was lower in 2010 and 2012 than in the other years.

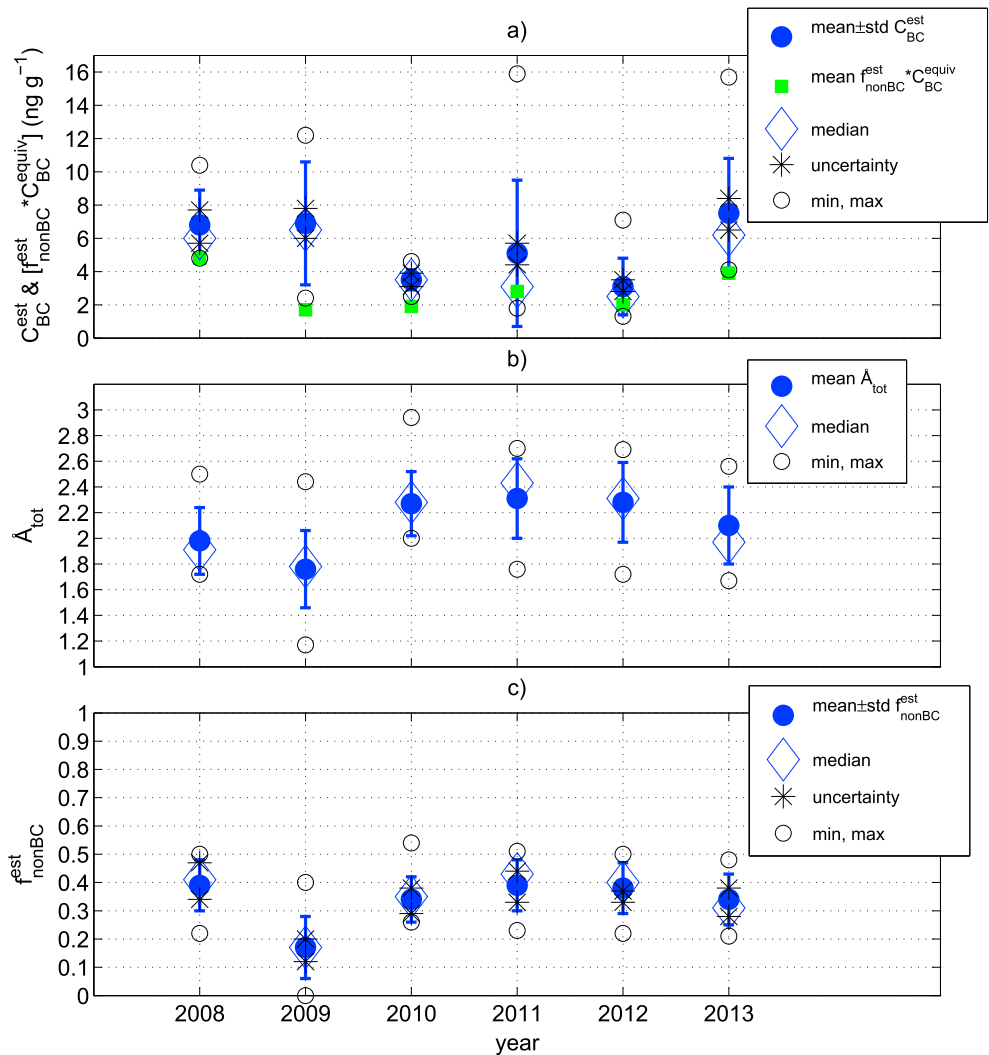


Figure 3. Means with standard deviations (1 sigma; error bars), medians, minimum, and maximum values and the uncertainty ranges of the means across all samples within a given year (Table 1 and Figure 1) for (a) C_{BC}^{est} , (b) \hat{A}_{tot} , and (c) f_{non-BC}^{est} . Also shown in Figure 3a is the mean across all samples of $f_{non-BC}^{est} \times C_{BC}^{equiv}$. This is a metric for particulate light absorption by non-BC components, expressed as an equivalent BC mass mixing ratio, and it can be directly compared to the mean value of C_{BC}^{est} as a measure of the relative roles of BC and non-BC absorption in snow darkening.

Variability in C_{BC}^{est} is smaller in 2010 than in the other years. While there were more samples in 2010 (24; Table 1) than in 2008 (7), 2009 (11), or 2011–2013 (11, 13, and 11), the range in C_{BC}^{est} (open circles in Figure 3a) is much smaller, as is the standard deviation. The 2010 samples are well distributed geographically around the Switchyard region (Figure 1), so this consistency cannot be attributed to spatial sampling bias in 2010 versus other years.

Comparison of the mean to the median, or the standard deviation to the range, (Figure 3a) within a given year shows that C_{BC}^{est} is not normally distributed. In all years except 2010, the mean is higher than the median, indicating that average snow mixing ratios are driven up by a “tail” of high C_{BC}^{est} samples (Figure 3 and Table 1).

In contrast, the absorption Ångström exponent is more normally distributed, so the mean and median of \hat{A}_{tot} are similar (Figure 3b). Annual mean \hat{A}_{tot} (Figure 3b) and f_{non-BC}^{est} (Figure 3c) in 2009 are lower than in other years. The lower value of \hat{A}_{tot} , which translates directly to a reduction in our estimate of the role of non-BC absorbers (lower f_{non-BC}^{est}), indicates a different type of source contributing to particulate light absorption in 2009 than in the other years.

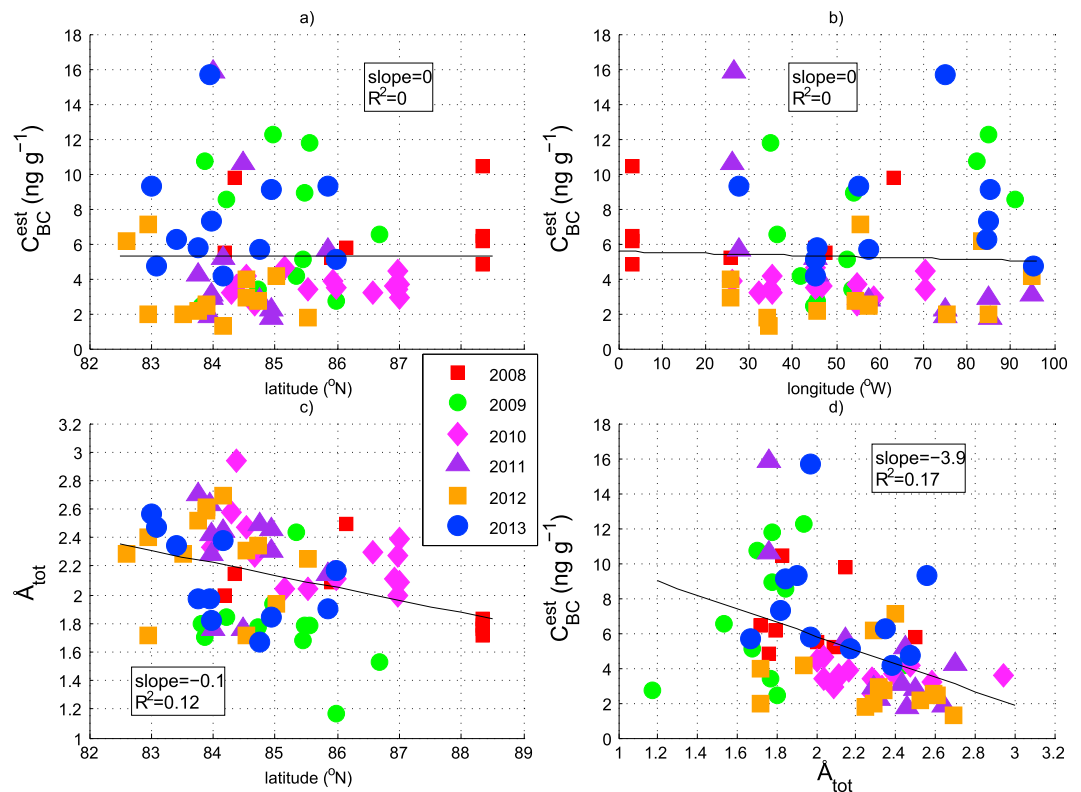


Figure 4. C_{BC}^{est} versus (a) latitude and (b) longitude, (c) \hat{A}_{tot} versus latitude, and (d) C_{BC}^{est} versus \hat{A}_{tot} for each sample listed in Table 1. Colored symbols (legend in Figure 4c) indicate the years of sampling. Linear fits to the data are shown.

Hegg *et al.* [2009, 2010] attributed absorption by particles in snow from a pan-Arctic set of samples to variable mixes of fossil fuel burning and biomass burning. That finding was based on chemical analysis of a subset of the Arctic snow samples of D10. Analyses using the same methods in northern China [Zhang *et al.*, 2013] and North America [Doherty *et al.*, 2014] found that dust and soil were also significant sources of snow particulate absorption, in addition to fossil fuel and biomass burning. The consistency of Hegg *et al.*'s [2009, 2010] finding across a large number of Arctic samples means that the particles in snow of the Switchyard region are also likely some mixture of aerosols from biomass burning and fossil fuel burning. Generally, combustion aerosol from fossil fuel burning is expected to be more black and less brown (lower \hat{A}_{tot}) than combustion aerosol from biomass burning (see D10 and references therein), although not categorically so. Indeed, this was usually, but not universally, the case for the Arctic samples jointly analyzed by D10 and Hegg *et al.* [2009, 2010]. We suggest that in our study region, the ratio of fossil fuel sources to biomass/biofuel sources was probably higher in 2009 than in the other years sampled.

Samples were not collected from the exact same locations in each year (Figure 1), so we investigated whether some of the variation in BC mixing ratios (C_{BC}^{est}) and the type of light-absorbing particles in snow (using \hat{A}_{tot} , or color, as a proxy) can be attributed to spatial gradients. Variations in C_{BC}^{est} do not correlate with either latitude (Figure 4a) or longitude (Figure 4b). However, \hat{A}_{tot} decreases with latitude by 0.1 per degree (Figure 4c). The correlation is significant ($p=0.003$) but small ($R^2=0.12$). \hat{A}_{tot} does not vary significantly with longitude (not shown; $R^2=0.03$, slope = 0.002). The strongest relationship is between C_{BC}^{est} and \hat{A}_{tot} (Figure 4d). While C_{BC}^{est} shows no dependence on \hat{A}_{tot} within a given sampling year, the data set overall does ($R^2=0.17$, $p=0.0004$). As noted above, the absorption Ångström exponent for combustion aerosol tends to be lower for fossil fuel than for biomass/biofuel sources. Thus, decreases in \hat{A}_{tot} are consistent with an increase in the ratio of fossil fuel to biomass burning aerosol, and in this region, this is also associated with higher mixing ratios of BC in snow.

The range in BC mixing ratios found here is consistent with that in two snow samples gathered near the North Pole (88.85°N, 175.43°W) in late April 2006, which were included in the Arctic survey of D10; these had C_{BC}^{est} of

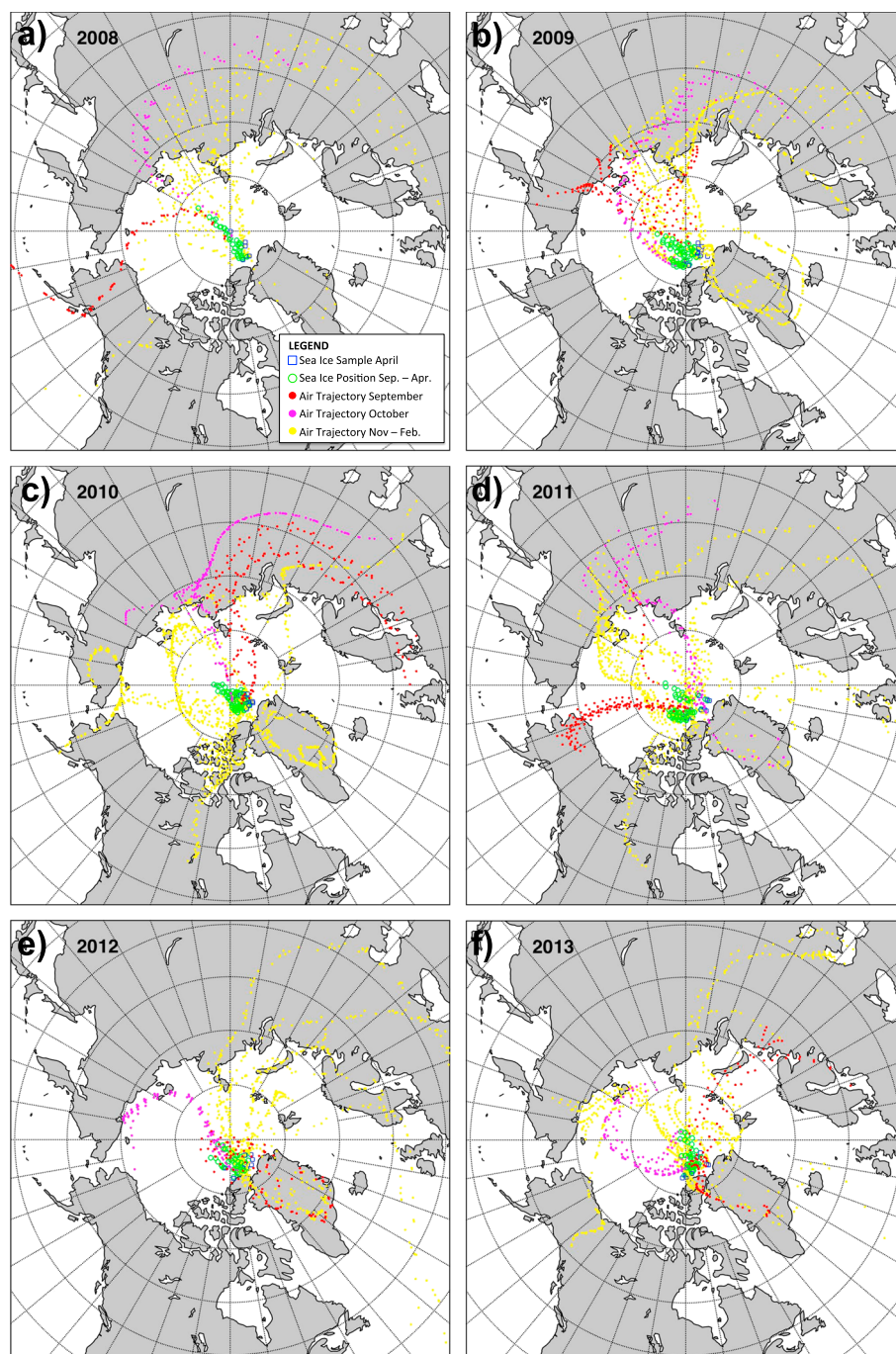


Figure 5. Composite results from September to February of sea ice location (blue and green) and the air mass locations (red, magenta, and yellow) for air originating at the surface of the sea ice for all sites sampled in the Switchyard region for (a) 2008, (b) 2009, (c) 2010, (d) 2011, (e) 2012, and (f) 2013.

5.3 ng g^{-1} and 8.3 ng g^{-1} . The Switchyard snow mixing ratios are somewhat lower than found at the northernmost Canadian sites of D10 (Sites 19–24, 75°N – 77°N , 255°W – 275°W) and the “Eureka” site (80.1°N , 273.3°W) shown in Figure 3 of D10. In Arctic Canada, $C_{\text{BC}}^{\text{est}}$ at different snow depths and sites varied from 2.5 to 18.5 ng g^{-1} , but most samples had $C_{\text{BC}}^{\text{est}}$ in the range of $5\text{--}12 \text{ ng g}^{-1}$ (median 8.7 ng g^{-1}). A_{tot} for those same samples varied from 1.8 to 3.4 (median 2.4) and showed no significant latitudinal gradient. While Hegg *et al.* [2009, 2010] found that for most Canadian sites biomass burning aerosol dominated snow

particulate light absorption, for the northernmost Canadian sites (Sites 19–24), fossil fuel and biomass burning sources were of comparable importance (Figure 7a of Hegg *et al.* (2010)). This is consistent with our inference of an increase in the ratio of fossil fuel to biomass burning sources for snow particulate absorption moving northward in the Switchyard region.

Interannual variations in C_{BC}^{est} and \dot{A}_{tot} presumably relate to changes in the source regions and histories of air masses reaching the sea ice over the lifetime of the snowpack. To see if there were any clear patterns between changes in air mass source region and variations in C_{BC}^{est} and \dot{A}_{tot} , we ran back trajectories for the months of September through February preceding sample collection. Back trajectories of sea ice drift starting at the sample location and going back to the prior September (the month with the highest climatological rate of snowfall on sea ice) were estimated using monthly gridded fields of sea ice motion produced by the International Arctic Buoy Programme [Rigor, 2005]. Back trajectories of air parcels for each month along these sea ice pathways were estimated by tracing parcels back 14 days through the monthly average National Centers for Environmental Prediction/National Center for Atmospheric Research Reanalyses 925 mb horizontal wind field [Kalnay *et al.*, 1996].

Air mass back trajectories for all samples 2008–2013 is shown in Figure 5. Most of the winter snowfall in this region—and therefore, most of the aerosol wet deposition—accumulates in September and October [Warren *et al.*, 1999, Figure 13]. The subsequent winter months are quite dry, with very little snowfall. Therefore, we have separately colored the air mass back trajectories from September to October (red and magenta, respectively) from all other months (shown in yellow). Given the long wintertime period with little snowfall, surface snow albedo in this region may be just as strongly influenced by aerosols that are dry deposited during winter and early spring as by wet deposition in the autumn snowfall.

In general, sea ice in the Switchyard region is formed north of eastern Siberia and is advected across the Arctic Ocean toward Greenland (green circles in Figure 5) in the Transpolar Drift Stream. Near-surface air at the sampled sea ice locations generally originates from Eurasia before crossing the ocean and reaching the sampling sites. Less frequently, air is transported to the region from Canada, Greenland, and the northeastern Atlantic Ocean. In the months of September and October, the air is particularly likely to have originated in the Eurasian (versus North American) side of the Arctic. None of the September–October air masses originate in the North Atlantic or Greenland/Iceland/Norwegian seas.

The year with the greatest variability in mixing ratios, 2011 (Figure 3a), also seems to have a large spread in the air mass back trajectories, although C_{BC}^{est} in 2009 and 2013 is nearly as variable and the back trajectories in those years do not stand out in this regard. Furthermore, the spread of air mass trajectories in 2010 is almost as large as in 2011, but C_{BC}^{est} in 2010 is the least variable—although, notably, for September and October (the months expected to dominate wet deposition), they are almost all associated with long-range transport from Eurasia. The low average \dot{A}_{tot} in 2009 (and to a lesser degree in 2008) may relate to the consistency with which air masses originate in western Russia and eastern Europe. However, it is likely that this analysis is confounded by the fact that it does not account for spatial and seasonal variations in emissions sources nor in removal of BC while in transit via precipitation and dry deposition. Including those variables in our analysis is beyond the scope of this project.

4. Conclusions

There was no trend in snow BC mixing ratios in the Switchyard region (82.6°N–88.3°N, 25°W–95°W) over the 2008 to 2013 period. Multiyear mean snow BC mixing ratios across the region were 3–6 ng g⁻¹, but mixing ratios at individual sites were as low as 1 ng g⁻¹ and as high as 16 ng g⁻¹. Variations in snow BC mixing ratios within the region showed no correlation with latitude or longitude; i.e., spatial variability is random. Simple back trajectory analyses for sea ice and air masses for the months of September through February preceding sampling did not reveal any clear relationships with variations in snow particulate mixing ratios or absorption Ångström exponents.

The observed variability suggests that for a representative comparison between observations and models, multiple samples need to be collected within a domain of, e.g., a climate model grid box. Furthermore, spatial variability within the Switchyard region in a given year is comparable to interannual variations in mixing ratios. Thus, in model/observation comparisons, it is likely just as critical to use spatially averaged observations as it is that the observational and model years match.

Although we lack ancillary chemical data to study the sources of light-absorbing particles in snow in the Switchyard region, previous Arctic studies indicate that particles likely originate from a mixture of fossil fuel and biomass/biofuel burning sources. The northward decrease in snow particulate absorption Ångström exponent suggests an increase in the ratio of fossil fuel to biomass/biofuel burning contributions to snow particulate light absorption. This is consistent with earlier findings in Arctic Canada (to the south and west of our study area), where fossil fuel sources of light-absorbing particles in snow were insignificant south of 75°N but became significant for sites at 75°N–77°N. For the Switchyard region, higher mixing ratios of BC in snow were generally associated with lower snow particulate absorption Ångström exponents, suggesting that fossil fuel emissions were the source of particles in the more polluted snow samples.

Acknowledgments

The full data set can be obtained by emailing the lead author sarahd@atmos.washington.edu. The data discussed in this study were collected as part of the NSF-sponsored "Switchyard" project, grant ARC-1022475, which was designed to study the circulation of sea ice and ocean in the Lincoln Sea and its connection with upstream and downstream conditions (<http://www.ideo.columbia.edu/Switchyard>, <http://psc.apl.washington.edu/switchyard/>). The analysis of the samples was supported by NSF grant ARC-06-12636 and EPA STAR grant RD-82503801. Most of the filtration was done in Greenland at the Kangerlussuaq International Science Center (KISS). We thank Kathy Young, the NSF manager at KISS, for providing laboratory space and a congenial working environment. Some of the snow samples were collected by Wendy Ermold and Matthew Alkire. This paper is JISAO contribution number 2473.

References

- Bond, T. C., et al. (2013), Bounding the role of black carbon in climate: A scientific assessment, *J. Geophys. Res. Atmos.*, *118*, 5380–5552, doi:10.1002/jgrd.50171.
- Boucher, O., et al. (2013), Clouds and aerosols, in *Climate Change 2013: The Physical Science Basis, Contrib. Work. Group I Fifth Assess. Rep. Intergov. Panel Clim. Change*, edited by T. F. Stocker et al., Cambridge Univ. Press, Cambridge, U. K., and New York.
- Clarke, A. D., and K. J. Noone (1985), Soot in the Arctic snowpack: A cause for perturbations in radiative transfer, *Atmos. Environ.*, *19*, 2045–2053.
- Clarke, A. D., K. J. Noone, J. Heintzenberg, S. G. Warren, and D. S. Covert (1987), Aerosol light absorption measurement techniques: Analysis and intercomparisons, *Atmos. Environ.*, *21*, 1455–1465.
- Conway, H., A. Gades, and C. F. Raymond (1996), Albedo of dirty snow during conditions of melt, *Water Resour. Res.*, *32*(6), 1713–1718, doi:10.1029/96WR00712.
- Dang, C., R. E. Brandt, and S. G. Warren (2015), Parameterizations for narrowband and broadband albedo of pure snow and snow containing mineral dust and black carbon, *J. Geophys. Res. Atmos.*, *120*, 5446–5468, doi:10.1002/2014JD022646.
- Doherty, S. J., S. G. Warren, T. C. Grenfell, A. D. Clarke, and R. Brandt (2010), Light-absorbing impurities in Arctic snow, *Atmos. Chem. Phys.*, *10*, 11,647–11,680, doi:10.5294/acp-10-11647-2010.
- Doherty, S. J., T. C. Grenfell, S. Forsström, D. L. Hegg, S. G. Warren, and R. Brandt (2013), Observed vertical redistribution of black carbon and other light-absorbing particles in melting snow, *J. Geophys. Res. Atmos.*, *118*, 5553–5569, doi:10.1002/jgrd.50235.
- Doherty, S. J., C. Dang, D. A. Hegg, R. Zhang, and S. G. Warren (2014), Black carbon and other light-absorbing particles in snow of central North America, *J. Geophys. Res. Atmos.*, *119*, 12,807–12,831, doi:10.1002/2014JD022350.
- Dou, T., C. Xiao, D. T. Shindell, J. Liu, J. Ming, and D. Qin (2012), The distribution of snow black carbon observed in the Arctic and compared to the GISS-PUCCINI model, *Atmos. Chem. Phys.*, *12*, 7995–8007, doi:10.5194/acp-12-7995-2012.
- Flanner, M. G., C. S. Zender, J. T. Randerson, and P. J. Rasch (2007), Present-day climate forcing and response from black carbon in snow, *J. Geophys. Res.*, *112*, D11202, doi:10.1029/2006JD008003.
- Gloersen, P., W. J. Campbell, D. J. Cavalieri, J. C. Comiso, C. L. Parkinson, and H. J. Zwally (1992), *Arctic and Antarctic Sea Ice, 1978–1987: Satellite Passive-Microwave Observations and Analysis*, 290 pp., NASA SP-511, Natl. Aeronaut. Space Adm., Washington, D. C.
- Gong, S. L., T. L. Zhao, S. Sharma, D. Toom-Sauntry, D. Lavoue, X. B. Zhang, R. Leaitch, and L. A. Barrie (2010), Identification of trends and interannual variability of sulphate and black carbon in the Canadian High Arctic: 1981 to 2007, *J. Geophys. Res.*, *115*, D07305, doi:10.1029/2009JD012943.
- Grenfell, T. C., S. J. Doherty, A. D. Clarke, and S. G. Warren (2011), Spectrophotometric determination of absorptive impurities in snow, *Appl. Opt.*, *50*(14), 2037–2048.
- Hegg, D. A., S. G. Warren, T. C. Grenfell, S. J. Doherty, T. V. Larson, and A. D. Clarke (2009), Source attribution of black carbon in snow, *Environ. Sci. Technol.*, *43*(11), 4016–4021, doi:10.1021/es803623f.
- Hegg, D. A., S. G. Warren, T. C. Grenfell, S. J. Doherty, and A. D. Clarke (2010), Sources of light absorbing aerosol in arctic snow and their seasonal variability, *Atmos. Chem. Phys.*, *10*, 923–10,938, doi:10.5194/acp-10-10923-2010.
- Jiao, C., et al. (2014), An AeroCom assessment of black carbon in Arctic snow and sea ice, *Atmos. Chem. Phys.*, *14*, 2399–2417, doi:10.5194/acp-14-2399-2014.
- Kalnay, E., et al. (1996), The NCEP/NCAR 40-year reanalysis project, *Bull. Am. Meteorol. Soc.*, *77*, 437–470.
- Lee, Y. H., et al. (2013), Evaluation of preindustrial to present-day black carbon and its albedo forcing from Atmospheric Chemistry and Climate Model Intercomparison Project (ACCMIP), *Atmos. Chem. Phys.*, *13*, 2607–2634, doi:10.5194/acp-13-2607-2013.
- Lund, M. T., and T. Berntsen (2011), Parameterization of black carbon aging in the OsloCTM2 and implications for regional transport to the Arctic, *Atmos. Chem. Phys.*, *11*(12), 32,499–32,534.
- Qian, Y., H. Wang, R. Zhang, M. G. Flanner, and P. J. Rasch (2014), A sensitivity study on modeling black carbon in snow and its radiative forcing over the Arctic and Northern China, *Environ. Res. Lett.*, *9*, doi:10.1088/1748-9326/9/6/064001.
- Rigor, I. G. (2005), Interdecadal variations in Arctic sea ice, PhD dissertation, 100 pp., Univ. of Washington, Seattle.
- Schwarz, J. P., R. S. Gao, A. E. Perring, J. R. Spackman, and D. W. Fahey (2013), Black carbon aerosol size in snow, *Sci. Rep.*, *3*, 1356, doi:10.1038/srep01356.
- Skeie, R. B., T. Berntsen, G. Myhre, C. A. Pedersen, J. S. Om, S. Gerland, and J. A. Ogren (2011), Black carbon in the atmosphere and snow, from pre-industrial times until present, *Atmos. Chem. Phys.*, *11*(11), 7469–7534, doi:10.5194/acp-11-6809-2011.
- Steele, M., J. Morison, W. Ermold, I. Rigor, M. Ortmeier, and K. Shimada (2004), Circulation of summer Pacific halocline water in the Arctic Ocean, *J. Geophys. Res.*, *109*, doi:10.1029/2003JC002009.
- Warren, S. G., and W. J. Wiscombe (1980), A model for the spectral albedo of snow. II: Snow containing atmospheric aerosols, *J. Atmos. Sci.*, *37*(12), 2734–2745.
- Warren, S. G., I. G. Rigor, N. Untersteiner, V. F. Radionov, N. N. Bryazgin, Y. I. Aleksandrov, and R. Colony (1999), Snow depth on Arctic sea ice, *J. Clim.*, *12*, 1814–1829.
- Xu, B., J. Cao, D. R. Joswiak, X. Liu, H. Zhao, and J. He (2012), Post-depositional enrichment of black soot in snow-pack and accelerated melting of Tibetan glaciers, *Environ. Res. Lett.*, *7*, doi:10.1088/1748-9326/7/1/014022.
- Zhang, R., D. A. Hegg, J. Huang, and Q. Fu (2013), Source attribution of insoluble light-absorbing particles in seasonal snow across northern China, *Atmos. Chem. Phys.*, *13*, 6091–6099, doi:10.5194/acp-13-6091-2013.